IOPscience iopscience.iop.org

Home Search Collections Journals About Contact us My IOPscience

Propagating and confined vibrational excitations in quasicrystals

This article has been downloaded from IOPscience. Please scroll down to see the full text article.

1993 J. Phys.: Condens. Matter 5 2489

(http://iopscience.iop.org/0953-8984/5/16/008)

View the table of contents for this issue, or go to the journal homepage for more

Download details:
IP Address: 171.66.16.96
The article was downloaded on 11/05/2010 at 01:17

Please note that terms and conditions apply.

J. Phys.: Condens. Matter 5 (1993) 2489–2510. Printed in the UK

Propagating and confined vibrational excitations in quasicrystals

J Hafner and M Krajčí†

Institut für Theoretische Physik, TU Wien, Wiedner Hauptstraße 8-10, A-1040 Wien, Austria

Received 16 December 1992, in final form 1 February 1993

Abstract. We present detailed investigations of vibrational modes in a hierarchy of rational (or commensurate) approximants to icosahedral quasicrystals, based on exact diagonalization of the dynamical matrix and recursion calculations of the vibrational spectrum. Our results demonstrate the existence of well defined longitudinal and transverse acoustic modes with isotropic dispersion relations in the vicinity of quasiperiodically distributed special points in wavenumber space, the 'Γ points' of the reciprocal quasilattice. Stationary eigenmodes are found around other high-symmetry points in reciprocal space corresponding to quasi-Brillouin zone boundaries. We show that strictly localized ('confined') modes exist and that their origin is a local topological frustration, i.e. in a local deviation from ideal icosahedral packing.

1. Introduction

For several decades it has been known that there are phases of condensed matter intermediate between periodic crystals and topologically disordered materials, in the sense that they show a diffraction pattern with sharp δ-peaks, but no translational symmetry. In this case the diffraction vectors are of the form

$$Q = \sum_{n=1}^{N} b_n a_n^*$$

with $N > 3$, i.e. the diffraction pattern may be indexed by integer indices, but only in a basis where the dimension is higher than that of the physical space. The first examples were the incommensurate phases, but the more recently discovered quasicrystals [1] excited more interest because the point-group symmetry of the diffraction pattern is a non-crystallographic group, like the icosahedral group with twelve fivefold axes.

Many physical properties of the condensed phases are closely related to the spectrum of the Hamiltonian. Of particular interest are the density of states and the behaviour of the wavefunctions (localized, extended, chaotic and so on). Are the eigenstates of the quasiperiodic Hamiltonian extended, as in crystals, or localized, as in amorphous solids when the disorder exceeds a critical value? The properties of the eigenstates will depend on two characteristic properties of the quasiperiodic lattices: one is their non-periodicity and the other is expressed by the Conway theorem [2]. This theorem states that any finite section of a quasicrystal will be repeated quasiperiodically an infinite number of times. The non-periodicity will cause the eigenstates to be localized, while the Conway theorem

† On leave of absence from Institute of Physics, Slovak Academy of Sciences, Bratislava CS-84228, ČSFR.

0953-8984/93/162489+22$07.50 © 1993 IOP Publishing Ltd

leads to extended states. In essence, this scenario has been confirmed by calculations of the eigenstates of one-dimensional (1D) quasilattices [3–6]. It was shown that most eigenstates are critical, i.e. neither extended nor localized, and that the power-law decay of the eigenstates is caused by the competition between non-periodicity and self-similarity.

Less is known about the spectrum and the eigenstates of two- and three-dimensional quasicrystals. One of the reasons is that the renormalization-group analysis of 1D quasiperiodic chains cannot be extended to higher-dimensional systems. This means that investigations of the eigenspectrum have to rely on numerical calculations. Numerical studies, however, can be performed only for finite systems constructed such as to approximate the infinitely extended quasicrystal as closely as possible. Most investigations concern 2D Penrose lattices with very simple model Hamiltonians. It has been shown that, unlike for the 1D quasicrystal, the density of states is not a Cantor set with a hierarchical gap structure, nor does it have large gaps [7]. However, in spite of the finite bandwidth, most of the eigenstates are critical and show a behaviour similar to power-law decay. It has also been shown that propagating eigenstates (i.e. states with a well defined wavevector) can exist in the vicinity of certain quasiperiodically arranged special points in wavenumber space [8–10] (the Γ points of the quasilattice) and that there can be strictly localized eigenstates associated with certain highly degenerate eigenvalues of the quasicrystal [11, 12].

The fundamental importance of the character of the eigenstates of quasiperiodic lattices has also stimulated many experimental investigations [13–17]. Here inelastic neutron-scattering measurements on single grains of icosahedral alloys are of particular importance because they allow one to study the dispersion relations of the collective excitations [15–17]. These studies confirm the existence of propagating phonon modes near strong Bragg peaks, with linear isotropic dispersion relations [15, 16]. In addition, halfway between strong Bragg peaks stationary points are found, corresponding to high-symmetry points at the boundary of a quasi-Brillouin zone.

In this paper we present an investigation of vibrational excitations in the icosahedral alloy Al–Zn–Mg. The model for the icosahedral structure is based on a three-dimensional Penrose tiling constructed using the projection method [18, 19] and the atomic decoration proposed by Henley and Elser [20]. The vibrational eigenstates are calculated for commensurate (or rational) approximants to the quasicrystal, both by straightforward diagonalization of the dynamical matrix and using a Lanczos-type recursion algorithm [21] for the determination of the vibrational density of states and the vibrational Bloch spectral functions. From the vibrational spectral function the dynamical structure factors and inelastic neutron scattering intensities may be calculated. The calculation of the spectral function confirms the existence of propagating collective excitations in the vicinity of the Bragg peaks of the quasilattice, for both longitudinal and transverse excitations. The spectral weight of these acoustic phonons scales with the intensity of the corresponding Bragg peak. While the acoustic modes show nearly linear dispersion, very weak dispersion is predicted for the higher-energy modes, especially in the vicinity of certain high-symmetry points in wavenumber space. The weak dispersion is compatible with an enhanced degree of localization of these modes.

The most direct information on the character of the eigenmodes comes from an explicit calculation of the eigenvectors of the dynamical matrix. The analysis of the eigenvectors allows one to identify several strictly localized eigenmodes and to establish a clear correlation between localization and a local frustration of icosahedral symmetry in the quasicrystal. However, due to the Conway theorem, these local modes are repeated infinitely often in the quasicrystal. Therefore, it may be more appropriate to speak of 'confined' instead of localized modes.

Our theoretical results show all the characteristic features detected in the experimental investigations [15–17] and offer a consistent explanation for these observations. Some preliminary results have been published in two short papers [12, 22].

2. Structural modelling

In the following we describe the structural modelling of the icosahedral Al–Zn–Mg alloy based on an atomic decoration of the 3D Penrose tiling, the construction of commensurate (or rational) approximants appropriate for the numerical calculation of the vibrational excitations, as well as the construction of the modulated quasicrystals where the atoms are in equilibrium under a given set of interatomic forces. We shall give only a brief outline; more details may be found in a previous publication [23].

2.1. Ideal quasicrystals

In the projection method [18, 19, 23, 24], the 3D Penrose lattice is generated by projecting a 'strip' of a 6D hypercubic lattice L_6 onto the physical space E_3. The strip is defined by extending a unit cube in L_6 parallel to E_3. The orientation of E_3 is defined in such a way that the projection of a star of orthogonal basis vectors in L_6 forms an icosahedral basis in E_3, $e_l = C(0, 1, \tau)$ + cyclic permutations (CP), $l = 1, 2, 3$; $e_l = C(0, -1, \tau)$ + (CP), $l = 4, 5, 6$ where $\tau = (1 + \sqrt{5})/2$ is the golden mean and C is a constant normalizing the basis vectors to unity. The projection of a 6D unit cube onto the 3D-space E_3' perpendicular to E_3 is a rhombic triacontahedron, the acceptance domain for vertices of the quasilattice. A vertex of L_6 belongs to the quasilattice only if its projection onto E_3' falls into the acceptance domain.

For the icosahedral alloys of the Al–Zn–Mg class the rhombohedral units (prolate (PR) and oblate (OR) rhombohedra) are decorated as proposed by Henley and Elser [20]: Al or Zn atoms occupy the vertices and the mid-points of all edges of the structural units, two Mg atoms are placed along the trigonal axis of each PR. A special composite unit is the rhombic dodecahedron (RD) formed by two OR and two PR. A decoration has been proposed for the fourfold vertex within each RD: four Mg atoms are placed on the edges originating from this vertex; altogether eight Mg atoms form a slightly distorted hexagonal bipyramid inside a RD.

2.2. Commensurate quasicrystals

A commensurate (or rational) approximant to the quasicrystal is obtained if, in the icosahedral basis in E_3', $e'_l = C'(0, -\tau, -1)$ + (CP), $l = 1, 2, 3$; $e'_l = C'(0, \tau, 1)$ + (CP), $l = 4, 5, 6$, the golden mean τ is replaced by a rational number $\tau_n = F_{n+1}/F_n$, where the F_n are Fibonacci numbers ($F_0 = 0$, $F_1 = 1$, $F_{n+1} = F_n + F_{n-1}$). The icosahedral basis in E_3 is unchanged. The triacontahedral acceptance domain is deformed, but its topology remains unchanged. The lattice created by this projection is a periodic Penrose lattice (PPL) with cubic symmetry [23, 24]. The lattice parameter of the cubic cell is $a_n = \sqrt{2 + 2/\sqrt{5}}\tau^n a_R$ where a_R is the length of the edge of a rhombohedral structural unit. The number of constituent rhombohedra is $N_R = 4F_{3n+3}$. We shall denote the commensurate approximants by F_{n+1}/F_n, the pair of the Fibonacci numbers corresponding to the approximation τ_n to the golden mean τ. For the lowest-order approximants, 1/1, 2/1, 3/2 and 5/3, the number of rhombohedra (equal to the number of vertices) is $N_R = 32$, 136, 576 and 2440, with the Henley–Elser decoration this corresponds to $N_{at} = 162$, 688, 2920 and 12380 atoms in the

cubic cell, respectively. Note that the 1/1 approximant is identical to the $(Al, Zn)_{49}Mg_{32}$ Frank–Kasper phase [25] and that very recently the 3/2 approximant of icosahedral Al–Zn–Mg was observed experimentally during crystallization of the metastable quasicrystal [26].

2.3. Modulated quasicrystals

In an infinitely extended quasicrystal the environment of each atomic site is unique. Hence, for a long-range potential, the forces acting, for example, on an Mg atom inside PR will be different in each PR. Therefore if one starts with a regular decorated Penrose tiling as a starting configuration and relaxes the system to a minimum of energy, one obtains a structure in which all atoms are displaced. This is illustrated in figure 1 for the example of the 5/3 approximant. However, if one calculates the Fourier transform of the relaxed configuration, one obtains a diffraction pattern with the same point-group symmetry as the ideal tiling itself. Therefore, the relaxed structure may be considered as a displacively modulated quasicrystal [23, 27].

In the present work, the relaxation has been performed using molecular dynamics (MD) and pseudopotential-derived interatomic forces [28]. For later use we note that the pseudopotential-derived pair forces describe the phonon frequencies of the crystalline metals Al, Zn, Mg and of crystalline and amorphous Mg–Zn alloys with an accuracy of typically five per cent. The MD relaxation was started at room temperature. Then the system was cooled to very low temperature, and finally the equilibrium atomic sites were determined using a steepest-gradient energy minimization. For a detailed discussion of the displacively modulated structures, see [23].

2.4. Reciprocal quasilattices

To the 6D hypercubic lattice L_6 belongs a 6D reciprocal lattice L_6^*. A 3D reciprocal lattice for the quasicrystal is defined by a projection of L_6^* on 3D wavevector space [29]. Projections of high-symmetry points of L_6^* define special points of the 3D reciprocal quasilattice. Special

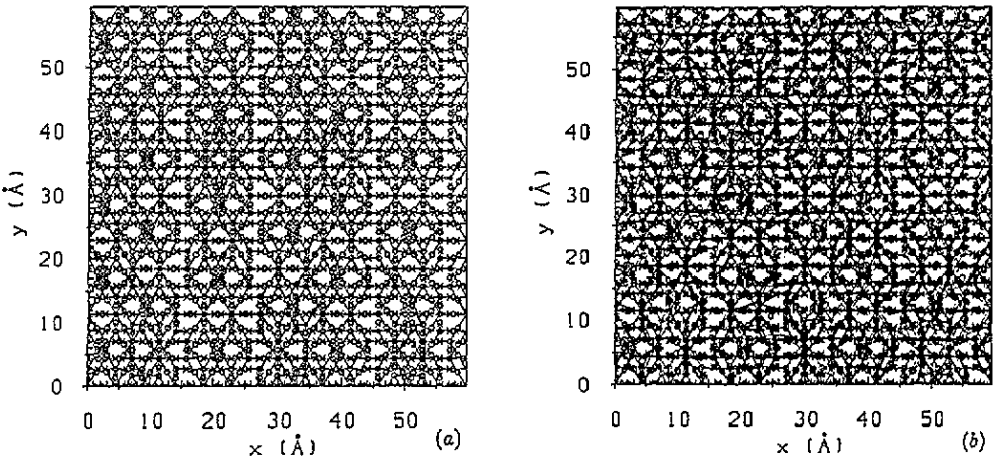

Figure 1. A projection of the ideal (*a*) and the displacively modulated (*b*) structure of the 5/3 approximant on the (x, y) plane. The edges of the Penrose tiles are drawn. Circles represent Al (Zn) atoms; crosses represent Mg atoms.

points are characterized by a generalized structure factor. Of particular interest are the Γ points, i.e. the projections of the (000000) points of the hypercubic lattice L_6^*. In this case, the generalized structure factor reduces to the conventional structure factor. Figure 2 shows the structure factor in a plane perpendicular to a twofold axis, calculated for the 5/3 approximant to icosahedral Al–Zn–Mg. The size of the spots is scaled with the square of the structure factor. This figure can be considered to represent a weighted distribution of the Γ points in wavenumber space. Two points should be noted. First, the structure factor is virtually discrete, although the reciprocal quasilattice is dense. Second, the structure factor is a quasiperiodic function in $\boldsymbol{k}$ space.

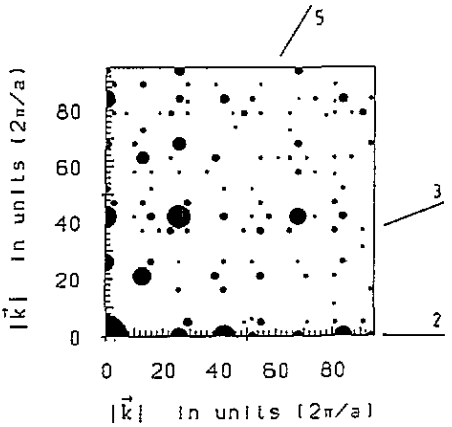

Figure 2. Structure factor for the 5/3 approximant to icosahedral Al–Zn–Mg in a plane perpendicular to a twofold axis. The size of each spot is proportional to the intensity of the Bragg peak. The wavevector $|\boldsymbol{k}|$ is given in units of $(2\pi/a)$, where $a = 59.82$ Å is the period of the approximant. The directions of the twofold, threefold and fivefold symmetry axes are marked.

In an icosahedral lattice there exist eight types of special points denoted as Γ, R, X_5, M_5, X_3, M_3, X_2, and M_2. Representative wavevectors are (in six-dimensional notation with h=1/2) (000000), (hhhhhh), (h00000), (0hhhhh), (hhh000), (000hhh), (hh0000), and (00hhhh), respectively. The point-group symmetry is the icosahedral group Y_h for Γ and R points, and D_{5d}, D_{3d} or D_{2h} for the other special points, according to whether the suffix is 5, 3 or 2, respectively. Graphical representations of the generalized structure factors associated with the special points are given by Niizeki and Akamatsu [29]. Here we only note that the generalized structure factor for the R point has intensities on the fivefold and threefold axis, but vanishes on the twofold axes, whereas the generalized structure factor for X_2 and M_2 points has intensities on the twofold axes, but not on the other symmetry axes.

3. Calculation of the vibrational eigenstates

The normal modes of vibration of a solid material (crystal, quasicrystal, glass) are given in the harmonic approximation in terms of the eigenvalues and eigenvectors of the real-space dynamical matrix

$$D\begin{pmatrix} ij \\ \alpha\beta \end{pmatrix} = \left(m_i^{-1/2} \Phi \begin{pmatrix} ij \\ \alpha\beta \end{pmatrix} m_j^{-1/2} \right) \tag{1}$$

determined by the atomic masses m_i and the force constant matrix Φ

$$\Phi\begin{pmatrix} ij \\ \alpha\beta \end{pmatrix} = \frac{1}{2} \frac{\partial^2}{\partial u_{i\alpha} \partial u_{j\beta}} \left(\sum_{\nu,\mu=A,B} \sum_{k(\nu)\neq l(\mu)} \sum_{l(\mu)} V_{\mu\nu}(|\boldsymbol{R}_k + \boldsymbol{u}_k - \boldsymbol{R}_l - \boldsymbol{u}_l|) \right) \tag{2}$$

given by the second derivative of the pair interaction energy with respect to the cartesian components $u_{i\alpha}$ of the displacements of the ith atom from its equilibrium position $\boldsymbol{R}_i$. In (2) the sum over $k(\nu)$ runs only over the sites $\boldsymbol{R}_k$ occupied by ν atoms. Here the dynamical matrix has been written for a binary alloy. As, according to all evidence, Al and Zn atoms are distributed at random in i-AlZnMg, we shall treat the quasicrystal as a pseudo-binary system, $A =$ Al or Zn, $B =$ Mg.

The $3N$ eigenmodes of an N-particle system are characterized by the eigenvalues ω_κ^2 and the eigenvectors $e_\kappa(\boldsymbol{R}_i)$ of the dynamical matrix.

3.1. Direct diagonalization

The straightforward approach consists in a direct diagonalization of the dynamical matrix. It is clear that this can be done only if the infinitely extended quasicrystal is replaced by a finite system. In our case we choose the commensurate quasicrystals with periodic boundary conditions. In this case, the dimension of the dynamical matrix is 486×486, 2064×2064 and 8760×8760 for 1/1, 2/1 and 3/2 approximants, respectively. It is clear that, even on present-day computers, direct diagonalization and calculation of all eigenvectors $e_\kappa(\boldsymbol{R}_j)$ will be possible only up to the 2/1 approximant. The vibrational density of states is then given in terms of the statistics of the eigenfrequencies:

$$n(\omega) = \sum_\kappa \delta(\omega - \omega_\kappa). \tag{3}$$

The character of the eigenstates is described by the participation ratio P [30]:

$$P(\omega_\kappa) = \left(\sum_j \frac{|e_\kappa(\boldsymbol{R}_j)|^2}{M_j}\right)\left(N \sum_j \frac{|e_\kappa(\boldsymbol{R}_j)|^4}{M_j^2}\right)^{-1} \tag{4}$$

where $e_\kappa(\boldsymbol{R}_j)$ is the eigenvector of the mode κ for atom j with mass M_j. For an extended eigenstate $P \sim 1$, whereas for a strictly localized eigenstate P is of order $(1/N)$.

3.2. Vibrational Green functions

Experimentally, the information on the vibrational eigenmodes is contained in the differential scattering cross section per unit solid angle and energy. According to the van Hove scattering law, the coherent cross section is proportional to the scattering function or dynamical structure factor $S(\boldsymbol{k}, \omega)$ [31]:

$$\frac{\mathrm{d}^2\sigma}{\mathrm{d}\Omega \mathrm{d}\omega} = \langle b \rangle^2 \left|\frac{k_{\mathrm{out}}}{k_{\mathrm{in}}}\right| S(\boldsymbol{k}, \omega) \tag{5}$$

where $\boldsymbol{k}$ is the wavevector difference between the incoming and scattered neutron, and b is the scattering length of the nucleus; $S(\boldsymbol{k}, \omega)$ may be expressed in terms of displacement–displacement correlation functions: in a one-phonon approximation we have [32]

$$S(\boldsymbol{k}, \omega) = \mathrm{e}^{-2W(k)} \sum_{i,j} \mathrm{e}^{-\mathrm{i}\boldsymbol{k}(\boldsymbol{R}_i - \boldsymbol{R}_j)} \int_{-\infty}^{\infty} \mathrm{d}t\, \mathrm{e}^{\mathrm{i}\omega t} \sum_{\alpha\beta} \langle k_\alpha u_{i\alpha}(t)\, k_\beta u_{j\beta}(0) \rangle. \tag{6}$$

Here $\exp(-2W)$ is the Debye–Waller factor and $\boldsymbol{u}_i(t)$ is the displacement of ith atom from its equilibrium position at time t. The angular brackets indicate thermal averaging.

The displacement–displacement correlation functions may be calculated in terms of the vibrational Green functions $G_{\alpha\beta}(ij, \omega^2)$ ($n(\omega)$ is the Bose occupation function)

$$\int_{-\infty}^{\infty} \mathrm{d}t\, \mathrm{e}^{\mathrm{i}\omega t} \langle u_{i\alpha}(t) u_{j\beta}(0) \rangle = -2\hbar[n(\omega) + 1]\, \mathrm{Im} G_{\alpha\beta}\big(ij, (\omega + \mathrm{i}\delta)^2\big) \tag{7}$$

the $G_{\alpha\beta}(ij, \omega^2)$ being defined as the inverse of the resolvent operator:

$$G_{\alpha\beta}(ij, \omega^2) = \big(\omega^2 \delta_{ij}\delta_{\alpha\beta} - D_{\alpha\beta}(ij)\big)^{-1}. \tag{8}$$

Hence the central task is the calculation of the vibrational Green function. The recursion method proceeds by tridiagonalizing the dynamical matrix, a diagonal matrix element of the Green function $G_{\alpha\alpha}(ii, \omega^2)$ is then calculated in terms of an infinite continued fraction. For example

$$n_{i\alpha}(\omega) = -\frac{2\omega}{\pi} \lim_{\delta \to 0} \mathrm{Im}\, G_{\alpha\alpha}\big(ii, (\omega + \mathrm{i}\delta)^2\big) \tag{9}$$

defines a local density of states on the site i, for vibrations polarized along the α direction. A Bloch spectral function $f_e(\boldsymbol{k}, \omega)$ for vibrational states with wavevector $\boldsymbol{k}$ and polarization vector $\boldsymbol{e}$ may be defined as

$$f_e(\boldsymbol{k}, \omega) = -\frac{2\omega}{\pi} \lim_{\delta \to 0} \mathrm{Im} \frac{1}{N} \sum_{ij} \sum_{\alpha\beta} e_\alpha \mathrm{e}^{\mathrm{i}\boldsymbol{k}\cdot\boldsymbol{R}_i} G_{\alpha\beta}(ij, (\omega + \mathrm{i}\delta)^2) e_\beta \mathrm{e}^{\mathrm{i}\boldsymbol{k}\cdot\boldsymbol{R}_j} \tag{10}$$

i.e. as the diagonal element of the vibrational Green function in a Bloch state. In terms of the Bloch spectral function, the dynamical structure factor may be written as (note that $\boldsymbol{u}(\boldsymbol{R}_i) \propto \boldsymbol{e}_i / \sqrt{M_i}$)

$$S(\boldsymbol{k}, \omega) = \frac{\hbar}{M} \frac{n(\omega) + 1}{2\omega} \mathrm{e}^{-2W(\boldsymbol{k})} (\boldsymbol{e} \cdot \boldsymbol{k})^2 f_e(\boldsymbol{k}, \omega). \tag{11}$$

This shows that the neutron-scattering law may be calculated from the Bloch spectral functions. For a binary or pseudo-binary system, partial spectral functions $f_e^{\mu\nu}(\boldsymbol{k})$ may be defined by restricting the atomic displacements to the sites occupied by the atom of a particular type. Partial dynamical structure factors $S_{\mu\nu}(\boldsymbol{k})$ are obtained by multiplying the spectral functions with the thermal occupation and Debye–Waller factors:

$$S_{\mu\nu}(\boldsymbol{k}, \omega) = \hbar \frac{n(\omega) + 1}{2\omega} \frac{\mathrm{e}^{-W_\nu(\boldsymbol{k})}}{\sqrt{M_\nu}} \frac{\mathrm{e}^{-W_\mu(\boldsymbol{k})}}{\sqrt{M_\mu}} (\boldsymbol{e} \cdot \boldsymbol{k})^2 f_e^{\nu\mu}(\boldsymbol{k}, \omega). \tag{12}$$

The total dynamical structure factor is given in terms of a weighted average over the partial structure factors

$$\langle b \rangle^2 S(\boldsymbol{k}, \omega) = [c_A b_A^2 S_{AA}(\boldsymbol{k}, \omega) + 2\sqrt{c_A c_B} b_A b_B S_{AB}(\boldsymbol{k}, \omega) + c_B b_B^2 S_{BB}(\boldsymbol{k}, \omega)] \tag{13}$$

where the b_A, b_B, c_A and c_B are the scattering lengths and concentrations of the A and B atoms, respectively.

Alternatively, the partial dynamical structure factors may be recast in terms of partial dynamical structure factors $S_{\mathrm{NN}}(\boldsymbol{k}, \omega)$, $S_{\mathrm{NC}}(\boldsymbol{k}, \omega)$ and $S_{\mathrm{CC}}(\boldsymbol{k}, \omega)$ describing the dynamical

fluctuations in the number density (NN) and the concentration (CC), as well as the corresponding cross term [33]. The total dynamical structure factor is then given by

$$\langle b\rangle^2 S(\boldsymbol{k},\omega) = [\langle b^2\rangle S_{\mathrm{NN}}(\boldsymbol{k},\omega) + 2\Delta b\langle b\rangle S_{\mathrm{NC}}(\boldsymbol{k},\omega) + \Delta b^2 S_{\mathrm{CC}}(\boldsymbol{k},\omega)]. \tag{14}$$

In the present work, we have used the recursion method [21] to calculate the vibrational density of states and the partial spectral functions. The recursion method leads to a representation of these quantities in terms of an infinite continued fraction. Termination of the continued fraction after L levels leads to a spectrum consisting of L weighted δ functions. Various methods have been proposed to extrapolate the continued fraction to $L \rightarrow \infty$ and to produce a smooth spectrum. Here we use the 'termination' procedure proposed by Lucchini and Nex [34].

For a crystal, the δ function peaks of the spectral function at the poles of the resolvent operator define propagating collective excitations with wavevector $\boldsymbol{k}$, polarization e and frequency ω. In a recursion calculation, the termination of the continued fraction after L exact levels leads to a finite resolution of the spectrum. The resolution is given roughly by the width of the vibrational band divided by the number of exact levels. Here, we calculated the spectral functions for the 5/3 approximant with 12 380 atoms, using 50 recursion levels. The maximum frequency is about $\hbar\omega \approx 40$ meV, leading to a resolution better than 1 meV. Peaks in the spectral function that are well defined on this scale may be taken to represent propagating collective modes with a well defined $\boldsymbol{k}$ vector.

Besides the spectral function, we calculated the total and partial vibrational DOS, $n(\omega)$ and $n_\nu(\omega)$. The DOS may be calculated by averaging over a set of local DOS $n_{i\alpha}(\omega)$, but a more efficient procedure is to calculate the diagonal matrix element of the Green function for an incoherent vibrational state (i.e. for a state where the phase $\exp(\mathrm{i}\phi_i)$, $\phi_i \in (0, 2\pi)$) at site i is a random variable [35]. Again the statistics can be improved by taking an average over independent incoherent states; in our calculations we used between five and ten random states for each DOS. We note that we have used a similar technique to describe the dynamical properties of glassy alloys [35, 36].

4. Vibrational density of states

The vibrational DOS calculated using the recursion method for the 2/1, 3/2 and 5/3 approximant, together with the result obtained by exact diagonalization of the dynamical matrix for the 2/1-approximant is shown in figure 3(a). Figure 3(b) shows the decomposition of the DOS into the Al(Zn) and Mg contribution. The result obtained by exact diagonalization is in principle a series of δ functions. To allow a comparison with the recursion method calculation, the result is given in the form of a histogram with a bin-width of 1 meV, comparable to the resolution of the recursion calculation.

We find that the exact diagonalization confirms the result of the recursion calculations and that the DOS converges rapidly in the hierarchy of the approximants. If there is any systematic change at all, than it consists in a slight sharpening of the maxima in the DOS at 10, 16, 26 and 39 meV (the spiky structures at the upper band edge are associated with localized modes, see below). Similar characteristic maxima in the DOS have been found by Suck [4] in icosahedral Al–Cu–Li. The investigation of the spectral function will allow us to associate the DOS maxima with stationary states at the high-symmetry points of the quasi-Brillouin zone.

Investigations of the vibrational DOS for the 3D-PPL with spring-constant models using exact diagonalization for the interatomic forces have been presented by Los and Janssen

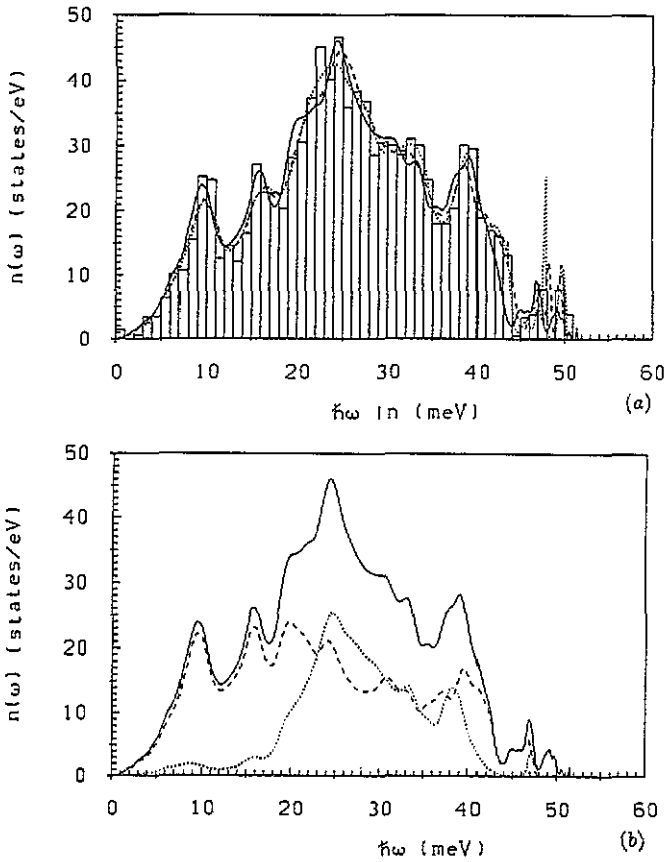

Figure 3. (*a*) Vibrational density of states for the 2/1 approximant (dotted curve), 3/2 (broken curve) and 5/3 approximant (full curve) to the icosahedral phase, calculated using the recursion method. The histogram shows the result obtained by exact diagonalization of the dynamical matrix for the 2/1-approximant. (*b*) Total and partial vibrational density of states for the 5/3 approximant. Full curve: total DOS; broken curve: Al(Zn); dotted curve: Mg.

[37]. They also find a rather rapid convergence of the DOS in a hierarchy of commensurate approximants, but for the undecorated Penrose lattice the structure of DOS is less pronounced. Los and Janssen also performed a calculation for a model structure for i-AlMn proposed by Janot and co-workers [38] and Lennard-Jones forces. The result is similar to that for the undecorated Penrose lattice, with a wide frequency region where $n(\omega) \propto \omega^2$, apart from small structures that can be interpreted in terms of van Hove singularities of the complex PPL. This result differs substantially from the DOS with well defined vibrational 'bands' predicted by our calculations for i-AlZnMg and from the neutron-scattering results of Suck and co-workers [13, 14, 39] for i-AlCuLi, i-AlPdMn and i-AlCuFe.

The decomposition of the vibrational DOS into the Al(Zn) and Mg contributions shows that the low-frequency part of the spectrum is dominated almost entirely by the vibrations of the Al(Zn) atoms decorating the framework of the Penrose lattice. The Al(Zn) motions also dominate the high-frequency end of the spectrum. The Mg vibrations are concentrated around the centre of the DOS.

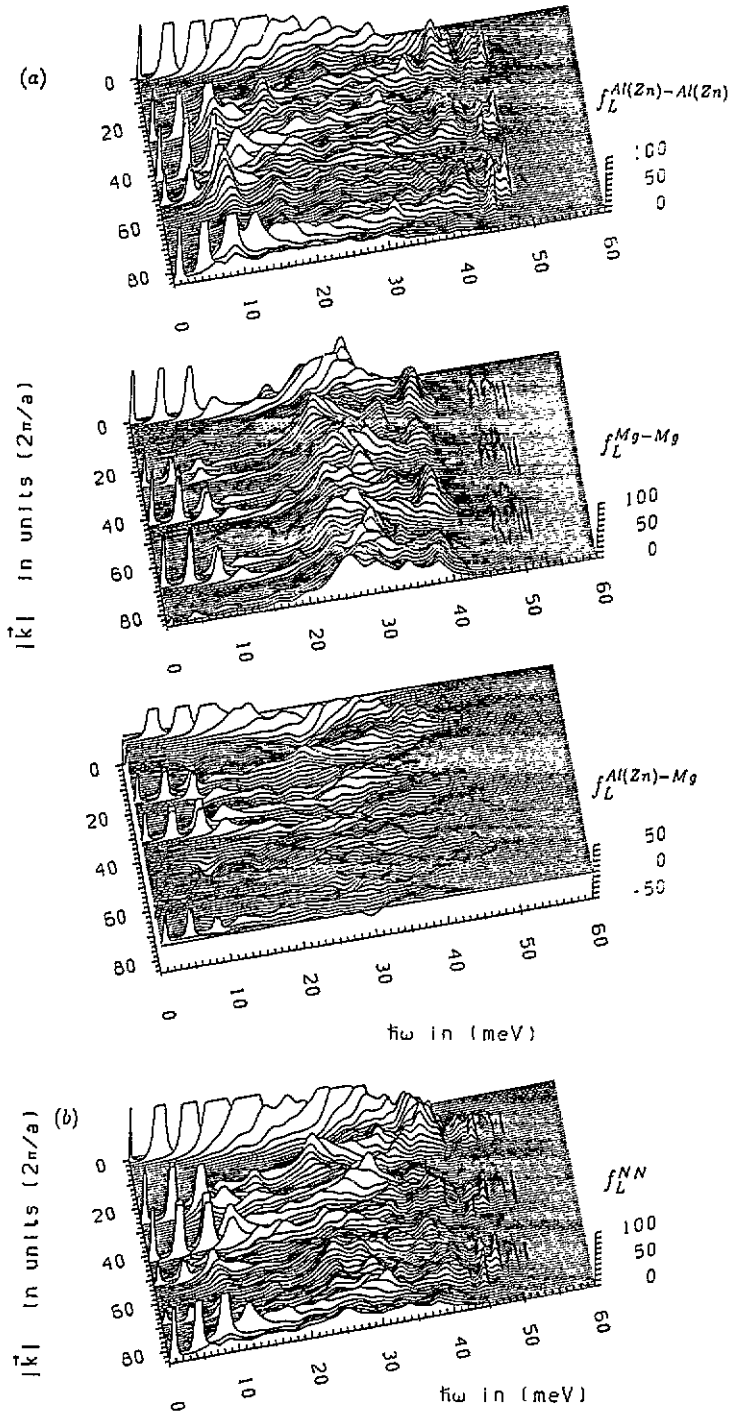

Figure 4. Partial vibrational spectral functions $f_L^{AB}(k,\omega)$, A, B=Al(Zn), Mg (*a*) for longitudinal excitations propagating in the direction of a twofold symmetry axis, calculated for the 5/3 approximant using the recursion method. (*b*) The partial Bhatia–Thorton spectral function $f_L^{NN}(k,\omega)$ for density fluctuation propagating in the same direction.

5. Vibrational spectral function

The partial vibrational spectral functions have been calculated for the 1/1, 2/1, 3/2 and 5/3 approximants. The results indicate a rapid convergence with increasing period of the approximant. Here we present only the results for the 5/3 approximant, where the characteristic structure is best observed. Figure 4(*a*) shows the partial spectral functions $f_L^{AB}(\boldsymbol{k},\omega)$ for longitudinal excitations propagating along a twofold symmetry axis (A = Al(Zn), B = Mg); (*b*) shows the Bhatia–Thornton partial spectral function for longitudinal density fluctuations, $f_L^{NN}(\boldsymbol{k},\omega)$, for $\boldsymbol{k}$ along the same symmetry direction. The spectral functions $f_L^{CC}(\boldsymbol{k},\omega)$ and $f_L^{NC}(\boldsymbol{k},\omega)$ for concentration fluctuations and coupled density and concentration fluctuations are not shown, because they have low amplitudes and only very little structure. The important result is the existence of several series of sharp inelastic peaks originating from the most intense Bragg peaks (the Γ points of the reciprocal quasilattice). These peaks represent propagating long-wavelength acoustic excitations ($\lambda = 2\pi/|\boldsymbol{q}|$, with $\boldsymbol{q} = \boldsymbol{k} - \boldsymbol{G}$, where $\boldsymbol{G}$ is the wavevector of the Γ point). For the density–density spectral function the intensity of these modes is proportional to the intensity of the Bragg peak (note that since $\bar{b}_{Al(Zn)} = 0.512 \times 10^{-12}$ cm and $b_{Mg} = 0.52 \times 10^{-12}$ cm [40], the density–density spectral function is almost identical to the weighted average for neutron scattering, cf. (18)). In the partial spectral functions the intensity of these modes is modulated according to the value of the partial static structure factor. The propagating longitudinal excitations are well defined for energies up to about 10 meV. At higher energies, the spectrum is much more complex, but there is still a pronounced $|\boldsymbol{k}|$ dependence of the vibrational frequencies. The Al(Zn) vibrations contribute to the entire band, whereas the intensity of the Mg vibrations is concentrated in the acoustic region and in the interval between 20–40 meV. The density–density spectral function describes essentially the dynamics of an average atom, the concentration–concentration spectral function describes out-of-phase vibrations of Al(Zn) and Mg atoms. The spectral function $f_L^{CC}(\boldsymbol{k},\omega)$ corresponds to special modes with rather high frequencies at the origin. However, the contribution of these modes to the total spectral intensity is rather small.

Figure 5 shows the partial spectral functions for transverse modes propagating along a twofold symmetry axis (the x direction) and polarized in the y direction. Again we find propagating collective excitations around the principal Bragg peaks, again with intensities proportional to those of the diffraction spots. Identical results are found for excitations polarized along the z direction.

Similar results are obtained for modes propagating in other symmetry directions. Figures 6 and 7 show the density–density spectral functions $f_L^{NN}(\boldsymbol{k},\omega)$ for $\boldsymbol{k}$ vectors along the fivefold and the threefold symmetry axis. Again, well defined acoustic modes are found around each Γ point. For wavevectors along the fivefold symmetry direction, the results are rather difficult to interpret, because close to the two most intense Bragg peaks relatively intense satellites are found (see figure 3). The acoustic modes originating from these closely spaced Γ points intersect each other, resulting in doubly peaked spectral functions. Along the threefold symmetry axis the Bragg peaks have only relatively low intensity (figure 2); this is reflected in the vibrational spectral functions (figure 7). The well defined peak at $|\boldsymbol{k}| = 30(2\pi/a)$ and $\hbar\omega \approx 10$ meV belongs to acoustic modes originating from an intense Γ point on the twofold symmetry axis. Finally, we show in figure 8 the density–density spectral function calculated along a general off-symmetry direction. This direction was determined as a vector equal to one third of the sum of vectors directed in twofold, threefold and fivefold symmetry directions. Propagating acoustic modes are found around the origin, but not at higher wavenumbers since there are no Γ points on this line. For very large $|\boldsymbol{k}|$

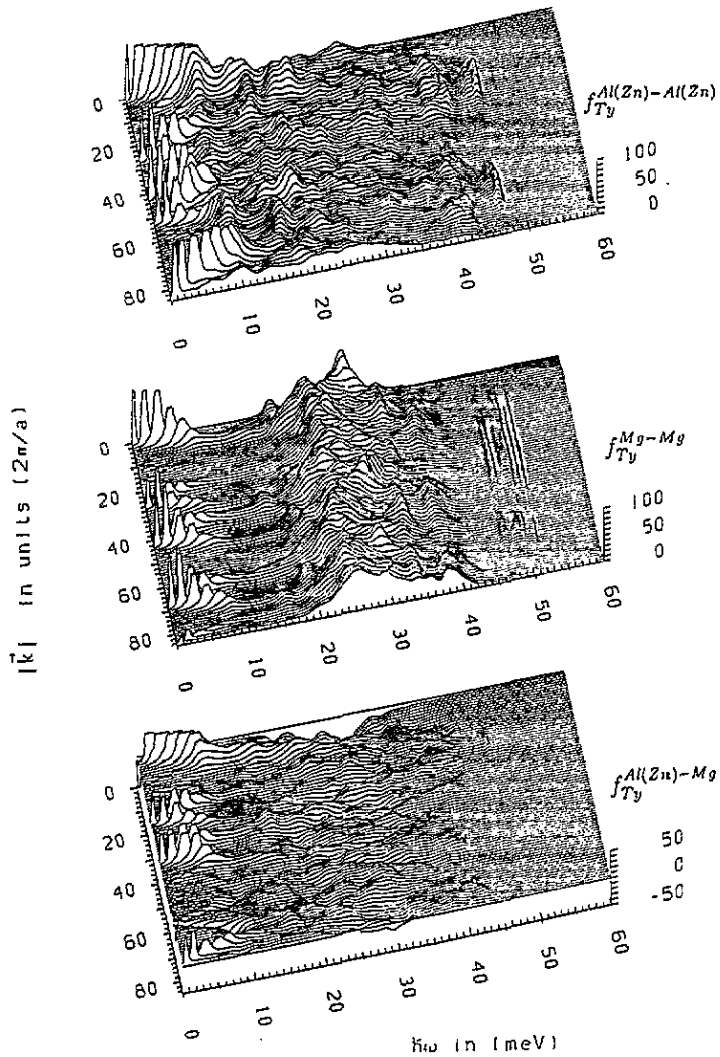

Figure 5. Partial vibrational spectral functions $f_{Ty}^{AB}(k,\omega)$, A, B =Al(Zn), Mg for wavevectors $k \parallel x$ (twofold symmetry axis) and polarization $e \parallel y$.

vector the spectral function approaches the form of the DOS. This is similar to amorphous alloys [35, 36]: very short-wavelength excitations resemble incoherent states, unless strong coherency effects appear, e.g. by umklapp scattering close to Γ points. The absence of sharply defined acoustic excitations for wavevectors oriented in off-symmetry directions explains the differences observed in the dynamical structure factors of polygrained [39] and single-grained [15, 16] quasicrystals.

6. Dispersion of collective excitations

Dispersion relations for collective excitations may be defined in terms of the positions of the peaks in the spectral functions. Here we use the density–density spectral functions to

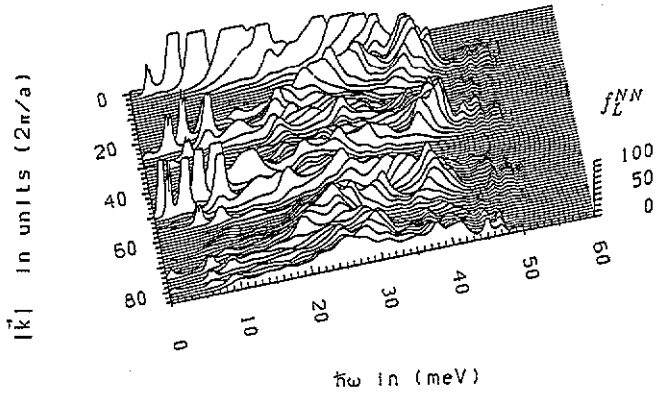

Figure 6. Density–density vibrational spectral function $f_L^{NN}(k, \omega)$ for longitudinal excitations with wavevectors along a fivefold symmetry axis.

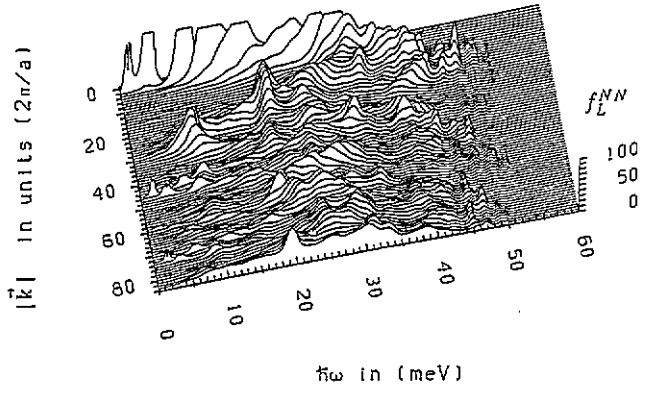

Figure 7. Same as figure 6, but for the k vector oriented along a threefold symmetry axis.

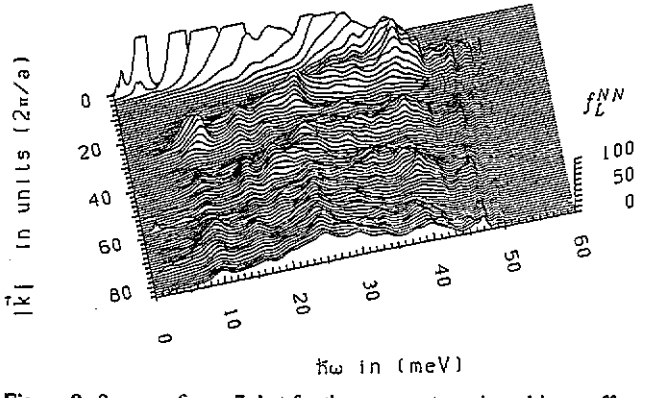

Figure 8. Same as figure 7, but for the wavevector oriented in an off-symmetry direction. See text.

define the dispersion relations. As f^{NN} is virtually identical to the total spectral functions calculated with the weights determined by concentration and neutron-scattering lengths (see

(18)), these dispersion relations should be representative for the results that can be obtained by inelastic neutron scattering. Figure 9 shows the dispersion relations for the longitudinal modes along the twofold and fivefold symmetry axes. Figure 10 shows the dispersion relations for the transverse excitations along a twofold symmetry axis. The results show a very characteristic pattern.

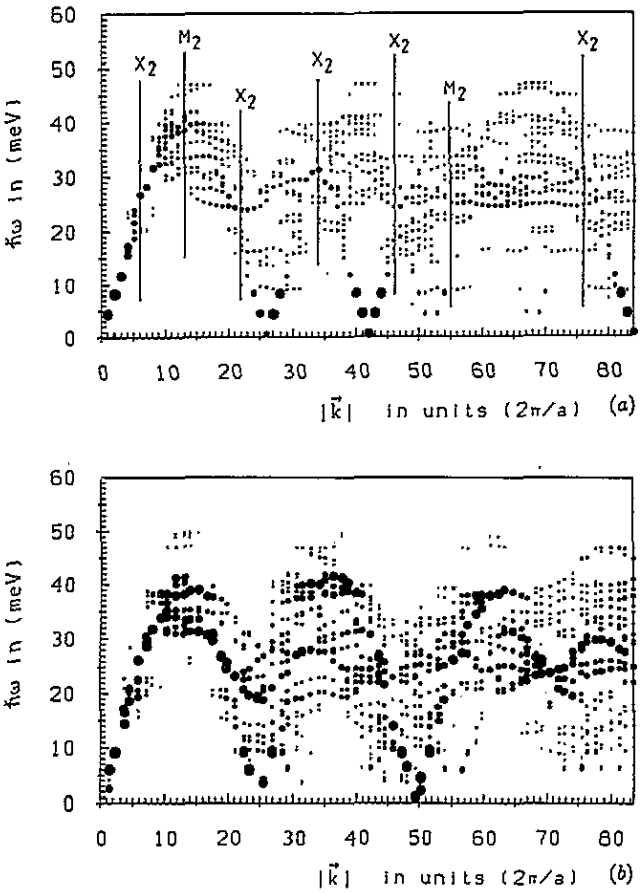

Figure 9. Dispersion relations for longitudinal collective excitations propagating along a twofold (*a*) and a fivefold (*b*) symmetry axis. A dot indicates the position of a peak in the spectral function; the size of the dot scales with the height of the peak. For the twofold axis the positions of the high-symmetry points X_2 and M_2 is marked.

First, around the Γ points the dispersion relation of both longitudinal and transverse excitations are linear to a very good accuracy. The slope of the dispersion relations is the same at each Γ point, independent of the direction of the wavevector and for transverse modes also independent of polarization. The longitudinal velocity of sound calculated from the slope of the dispersion relation is $c_L = 5.6 \times 10^5\,\mathrm{cm\,s^{-1}}$, the transverse velocity of sound $c_T = 2.4 \times 10^5\,\mathrm{cm\,s^{-1}}$. The prediction of isotropic dispersion relations for acoustic modes agrees very well with the neutron-scattering results of Goldman and co-workers [15, 16]. The elastic isotropy of the icosahedral alloy stems from the fact that the symmetry of the icosahedral point-group is higher than cubic [41].

Second, at higher energies the phonon dispersion relations are stationary around certain

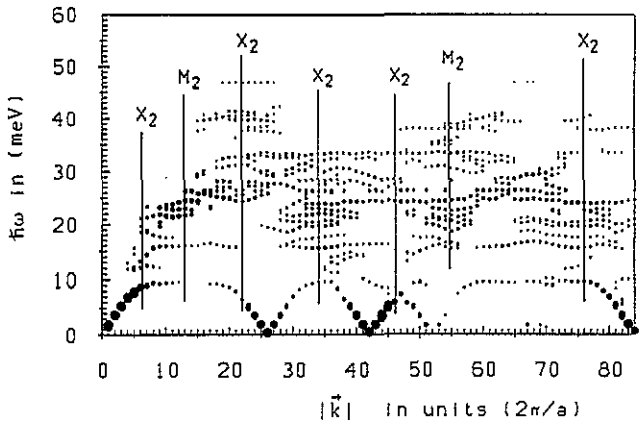

Figure 10. Dispersion relations for transverse collective excitations propagating along a twofold symmetry axis. Compare with figure 9

high-symmetry points of the reciprocal quasilattice. In addition, maxima of the dispersion relations are found at some of the Γ points. On the twofold symmetry axis there are X_2 and M_2 points. They are marked in figures 9(*a*) and 10. For all other symmetry points the intensity of the generalized structure factor is zero on the twofold axis [29]. On the fivefold axis possible symmetry points are R, M_5 and X_5. It is tempting to draw an analogy between the stationary dispersion relations at the special points of the quasilattice and the behaviour of phonon dispersion relations at the Brillouin zone boundary of crystals. In some cases a special point is situated just halfway between two Γ points and in this case the analogy seems to be complete. However, there are also special points that cannot be interpreted in this simple way, and we have to remember that the reciprocal quasilattice is dense.

Stationary modes are found at energies of about 10 meV, 16 meV, in the range 20–30 meV, and around 40 meV. Hence there is a clear correlation between the peaks in the vibrational DOS and the stationary modes.

7. Inelastic neutron scattering intensities

The total dynamical structure factor $S(\boldsymbol{k}, \omega)$ describing the intensity of inelastically scattered neutrons may be calculated by multiplying the vibrational spectral functions with the thermal occupation factor, the Debye–Waller factor (calculated from the partial DOS) and the square of the wavevector. Superposition of these partial dynamical structure factors according to (13) yields $S(\boldsymbol{k}, \omega)$. The total dynamical structure factor for $\boldsymbol{k}$ along a twofold symmetry axis is shown in figure 11. Compared to the spectral function, the factor k^2 minimizes the intensities at small wavevectors and the thermal occupation factor $(n(\omega)+1)/\omega$ (proportional to ω^{-2} at low temperatures) dampens the intensities at high frequencies. Therefore, intense inelastic peaks are found only around the most intense Bragg peaks. An enlarged version of the dynamical structure factor around the Bragg peak at $|\boldsymbol{k}| = 26(2\pi/a) = 2.73\,\text{Å}^{-1}$ is shown in figure 11(*b*). This shows that it will be very difficult to detect longitudinal inelastic excitations at wavevectors differing by more than $0.3\,\text{Å}^{-1}$ from a Γ point. For the transverse modes the damping effect is weaker due to the lower eigenfrequencies. However, since the local maxima are quite sharply defined, the dispersion relations derived from $S(\boldsymbol{k}, \omega)$ are almost identical to those derived from the peaks in the weighted spectral function $f(\boldsymbol{k}, \omega)$

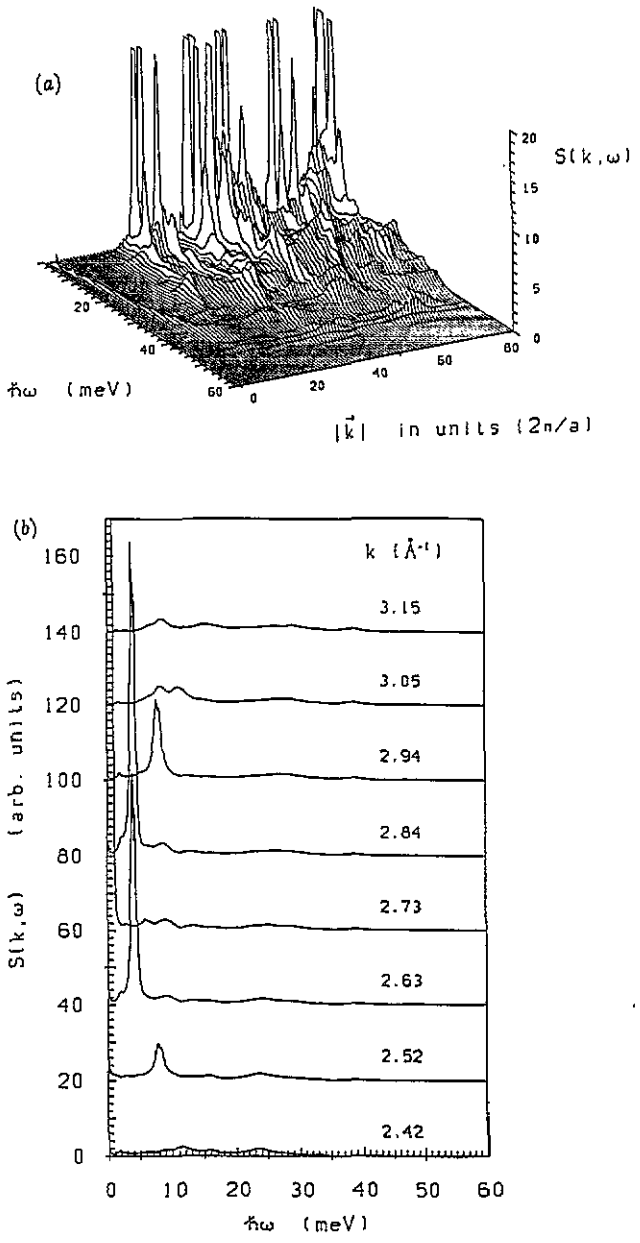

Figure 11. (*a*) Total dynamical structure factor $S(k, \omega)$ for longitudinal collective excitations propagating along a twofold symmetry direction. (*b*) Enlarged section of $S(k, \omega)$ around the Bragg peak at $|k| = 26.(2\pi/a) = 2.73\,\text{Å}^{-1}$. See text.

(which in the present case is almost identical to $f_{NN}(k, \omega)$). In this respect quasicrystals are similar to periodic crystals and different from glasses, where the multiplication of a broad spectral function with the thermal occupation function shifts the peak in $S(k, \omega)$ to lower frequencies compared to those in $f(k, \omega)$ [35,36].

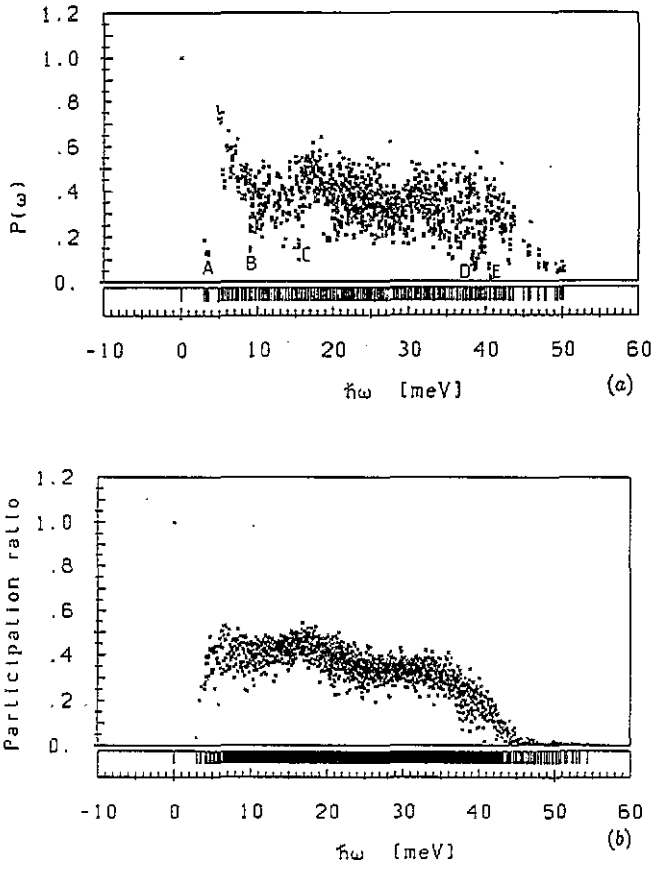

Figure 12. Participation ratio $P(\omega)$ of the vibrational eigenmodes for the 2/1 approximant to the Al–Zn–Mg quasicrystal (*a*), and for a 688-atom model of an amorphous Al–Zn–Mg alloy (*b*). The labels A–E refer to the some of the localized modes discussed in the text.

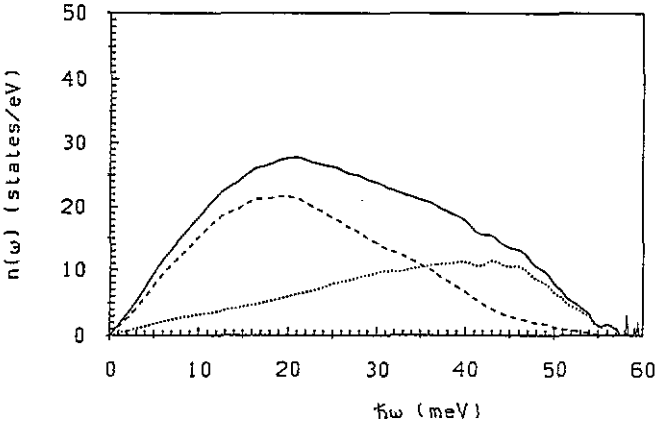

Figure 13. Vibrational density of states $n(\omega)$ for amorphous Al–Zn–Mg.

8. Confined vibrational modes

The character of the eigenmodes is characterized by the participation ratio $P(\omega)$, see (4). Figure 12(a) shows the participation ratio $P(\omega)$ for the eigenmodes of the 2/1 approximant calculated by exact diagonalization of the dynamical matrix. For comparison, figure 12(b) shows the participation ratio of a 688-atom model of an Al–Zn–Mg glass, prepared by a molecular dynamics quench and a subsequent steepest-descent energy minimization (details of the modelling algorithm, together with the atomic and electronic structure of amorphous Al–Zn–Mg, are described in [41]). The vibrational density of states of the glass (figure 13) covers about the same range of frequencies as that of the quasicrystal, but lacks the peaks corresponding to the stationary modes of the quasicrystal. The partial DOS shows a broad overlap between the Al(Zn) and Mg vibrations. The distribution of the participation ratios is distinctly different in the quasicrystalline and amorphous phases. In the glass, the participation ratios are scattered between $P(\omega) \sim 0.3$ and $P(\omega) \sim 0.5$ at intermediate frequencies and tend to zero at the upper edge of the band. The existence of high-frequency localized modes is easily understood in terms of strained local configurations characteristic for a disordered solid. Characteristically, the high-frequency modes are localized in sites with a high atomic level pressure [42, 43]. In addition, a few low-frequency localized modes are detected. The existence of low-frequency localized modes and the importance of these modes for understanding the interesting low-temperature thermodynamic properties of glasses have been much-debated subjects [44, 45]. The 'soft-potential model' for the origin of the localized modes enjoys a long-lived popularity, although attempts to associate the local modes with well defined atomic arrangements have met with only limited success [46].

Compared to the amorphous alloy, the participation ratios of the eigenmodes of the quasicrystal are more widely scattered and localized modes (defined somewhat arbitrarily by $P < P_c$, $P_c = 0.2$ for the 688-atom model) are found over the entire frequency range. For the quasicrystal we can establish a precise relation between local deviations from the icosahedral packing and at least some of the localized modes. Figure 14(a) shows the displacement pattern of the fifth eigenmode. Atoms are drawn at the equilibrium positions of the relaxed displacively modulated quasicrystal, arrows show the projections of the eigenvectors at each atomic site on the (x, y) plane. Figure 14(b) shows for comparison the idealized structure. The mode considered is one out of a group of eight eigenstates labelled 'A' in figure 12(a). In the ideal quasicrystal these modes would be degenerate, but the displacive modulation lifts the degeneracy. In these eigenmodes the atomic displacements are largest in four groups of eight atoms each. These 32 atomic positions are just the 13-fold coordinated sites in the 2/1 approximant (see figure 14(b)).

Note that, even though a quasicrystal has icosahedral point-group symmetry, this does not mean that all atomic sites have full icosahedral symmetry. Ideal icosahedral site-symmetry is characterized by coordination number twelve and a fivefold symmetry axis passing through the site. The local deviations from icosahedral symmetry in crystals, glasses and quasicrystals may be described in terms of a network of disclination lines [47]. 'S4' and 'S6' disclinations are defined to lie along bonds that are surrounded by four or six tetrahedra instead of five. These disclination lines characterize local deviations from icosahedral symmetry that exist even in ideal infinitely extended quasicrystals. They are not related to the phason defects introduced in the commensurate approximants. The 13-fold coordinated sites in a Penrose-lattice with Henley–Elser decoration (they are situated in mid-edge and vertex positions of the oblate rhombohedra) are links of seven (four S4 and three S6) respectively three (one S4 and two S6) disclinations. The high local density of

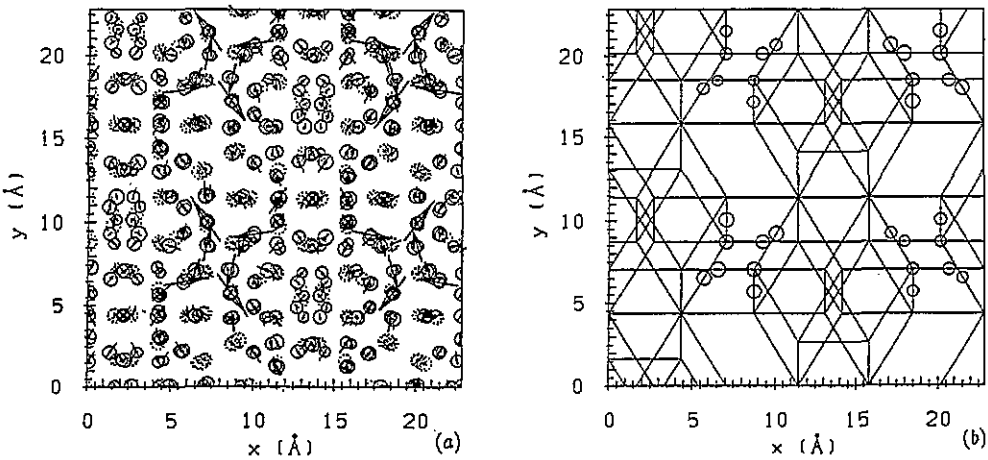

Figure 14. (*a*) Projection of the relaxed (displacively modulated) lattice of the 2/1 approximant on the (x, y) plane. The arrows show the eigenvectors of the localized fifth eigenmode (labelled 'A' in figure 12). The diameter of the circles representing the atoms is scaled with the z coordinate. (*b*) The 13-fold coordinated sites participating in the localized modes.

disclination lines indicates a high degree of frustration (in the sense of a deviation from ideal icosahedral packing). A high density of S4 disclinations is associated with a locally reduced packing density; it is therefore natural that the localized eigenstate is a low-frequency mode. Similar correlations between localization and topological frustration may be established for other groups of the eigenstates. For example, the modes labelled 'B' and 'C' in figure 12(*a*) are again associated with 13-fold coordinated sites. Certain high-frequency localized states (labelled 'D' and 'E' in figure 12) are associated with a high density of S6 disclinations. All Mg sites in the quasilattice have coordination $Z \geqslant 14$, those in the body diagonal of the prolate rhombohedra have $Z = 16$ and link four S6-disclinations. A high local density of S6 disclinations indicates a locally increased packing density and it is plausible that this leads to a localized high-frequency mode. This is shown in figure 15. In the eigenmode 1902 ($\hbar\omega = 40.65$ meV, $P(\omega) = 0.162$), only two pairs of atoms show large displacements from their equilibrium sites. These atoms are Mg atoms placed along the body diagonal of the prolate rhombohedra with coordination number $Z = 16$. Other sites of this type are involved in other localized high-frequency modes.

Although we have called eigenmodes with a low participation ratio 'localized' modes, these are not localized modes in a classical sense with an exponentially decaying envelope. According to Conway's theorem, the local configurations supporting these modes are repeated infinitely often in the quasicrystalline lattice. Hence the same eigenmode appears at many places in the quasilattice: it is not localized in the sense that the amplitude decays exponentially with distance from the centre of the mode, but it is confined to a well defined supporting structure. For this reason it appears to be more appropriate to speak of 'confined' eigenstates. We note that, for two different tight-binding models on 3D Penrose lattices such confined eigenstates have been identified and discussed by Krajčí and Fujiwara [11].

According to Conway's theorem, the number of confined modes should be proportional to the volume of the system. In an ideal infinite quasicrystal, the confined modes would be infinitely degenerate. In this context it is interesting to emphasize that the frequency of the most prominent confined modes is close to peaks or shoulders in the vibrational spectrum and that the height of these peaks increases with the order of the approximant.

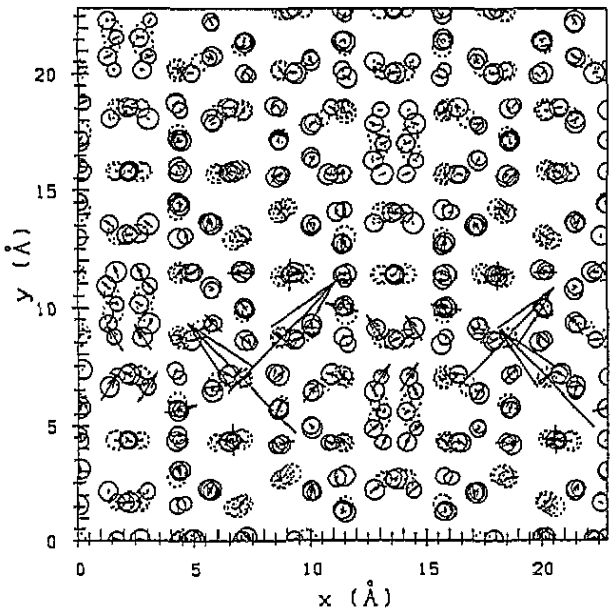

Figure 15. (*a*) Displacement pattern of a localized high-frequency mode (labelled 'E' in figure 12). See text.

For the lowest-order approximants, the confined modes contribute only a few per cent of the height of the peaks. Most of the states at this frequency are stationary states associated with high-symmetry points. The relation between confined and stationary states deserves further investigation.

We should also emphasize that the results obtained here refer only to a low-order commensurate approximant. With 688 atoms in the 2/1 approximant, there are 2064 vibrational eigenstates. This is of the same order of magnitude as the number of eigenstates in the Krajčí and Fujiwara one-band model of the 5/3 approximant to the 3D Penrose lattice with 2440 vertices. In the next generation of our model—the 3/2 approximant—there would be 8760 eigenstates. For such numbers, special techniques for diagonalizing very large matrices are required. Hence, for the time being, we cannot claim that confined eigenstates exist in infinite quasicrystals. However, the supporting structures of the confined states are not a consequence of the commensurate approximation, but exist in larger models and in infinite quasicrystals as well, and the existence of a variety of confined states may be expected.

9. Summary

We have presented the first investigation of collective excitations for a realistic model of a quasicrystal, using exact diagonalization of the dynamical matrix for low-order commensurate quasicrystals and using recursion calculations of the spectrum for very large models.

Our calculations show the existence of well defined propagating longitudinal and transverse modes ('phonons') around the quasiperiodically distributed Γ points. The slope of the dispersion relations is independent of the direction of the wavevector and for transverse modes is also independent of the direction of the polarization in the plane perpendicular to the wavevector. This shows that, as expected, the quasilattice is elastically isotropic.

At higher frequencies, we predict stationary vibrational modes around the special high-symmetry points of the reciprocal quasilattices. These stationary modes are associated with peaks ('quasi-van-Hove singularities') in the density of states.

These results are in very good agreement with recent inelastic neutron-scattering data on icosahedral Al–Cu–Li (calculations for this alloy are in progress). The phonon dispersion relations also show striking analogies with the dispersion relations of electrons in quasicrystals [10, 41].

We have shown that strictly localized ('confined') eigenstates can exist in commensurate quasicrystals and we have established a clear correlation between the confined modes and local topological frustrations of the ideal icosahedral packing. The supporting structures of the confined modes are not induced by the commensurate approximation; they exist also in the infinite quasicrystal. Hence confined modes may be expected even in real quasicrystals. Our results point to a correlation between the confined eigenstates and the stationary modes, whose precise nature must be left to future investigations.

Acknowledgments

This work has been supported by the Fonds zur Förderung der wissenschaftlichen Forschung in Österreich (Austrian Science Foundation) under project no. P8148-TEC.

References

[1] Steinhardt P J and Ostlund S (eds) 1987 *The Physics of Quasicrystals* (Singapore: World Scientific)
[2] Gardner M 1977 *Sci. Am.* **236** 110
[3] Kohomoto M and Sutherland B 1986 *Phys. Rev.* B **34** 3849
[4] Ashraff J A and Stinchcombe R B 1989 *Phys. Rev.* B **39** 2670
[5] Benoit C 1989 *J. Phys.: Condens. Matter* **1** 335
[6] Benoit C, Poussigue G and Azouragh A 1990 *J. Phys.: Condens. Matter* **2** 2519
[7] Tsunetsugu H, Fujiwara T, Ueda K and Tokihiro T 1991 *Phys. Rev.* B **43** 8879
[8] Patel H and Sherrington D 1989 *Phys. Rev.* B **40** 11185
[9] Ashraff J A, Luck J M and Stinchcombe R B 1990 *Phys. Rev.* **B41** 4314
[10] Hafner J and Krajčí M 1992 *Phys. Rev. Lett.* **68** 2321
[11] Krajčí M and Fujiwara T 1988 *Phys. Rev.* B **38** 12903
[12] Hafner J and Krajčí M 1993 *Phys. Rev.* B **47** 1084
[13] Suck J B, Bretscher H, Rudin H, Grütter P and Güntherodt H J 1987 *Phys. Rev. Lett.* **59** 102
[14] Suck J B, Janot C, de Boissieu M and Dubost M 1990 *Phonons '89* ed S Hunklinger, W Ludwig and G Weiss (Singapore: World Scientific) p 576
[15] Goldman A I, Stassis C, Bellisent R, Moudden H, Pyka N and Gayle F W 1991 *Phys. Rev.* B **43** 8763
[16] Goldman A I, Stassis C, de Boissieu M, Currat R, Janot C, Bellisent R, Moudden H and Gayle F W 1992 *Phys. Rev.* B **45** 10280
[17] Quillichini M, Heger G, Hennion B, Lefebvre S and Quivy A 1990 *J. Physique (Paris)* **51** 1785
[18] Elser V and Henley C L 1985 *Phys. Rev. Lett.* **55** 2883
[19] Bak P 1986 *Phys. Rev. Lett.* **56** 861
[20] Henley C L and Elser V 1986 *Phil. Mag. Lett.* **53** L59
[21] Heine V, Haydock R, Bullet D W and Kelly M J 1980 *Solid State Physics* **35** (New York: Academic)
[22] Hafner J and Krajčí M 1993 *Europhys. Lett.* **21** 31
[23] Krajčí M and Hafner J 1992 *Phys. Rev.* B **46** 10669
[24] Mihalkovič M and Mrafko P 1992 *J. Non-Cryst. Solids* **143** 225
[25] Bergmann G, Waugh J L T and Pauling L 1957 *Acta Crystallogr.* **10** 254
[26] Mukhopadhyay N K, Ishihara K N, Ranganathan S and Chattopadhyay K 1991 *Acta Metall.* **39** 1151
[27] Jansen T 1988 *Quasicrystalline Matterials* ed C Janot and J M Dubois (Singapore: World Scientific) p 327
[28] Hafner J 1987 *From Hamiltonians to Phase Diagrams* (Berlin: Springer)
[29] Niizeki K and Akamatsu T 1990 *J. Phys.: Condens. Matter* **2** 2759

[30] Bell R J and Dean P 1972 *Amorphous Materials* ed R W Douglas and B Ellis (New York: Wiley) p 443
[31] Lovesey S and Springer T (eds) 1977 *Dynamics of Solids and Liquids by Neutron Scattering* (Berlin: Springer)
[32] Maradudin A A, Motroll E W, Weiss G W and Ipatova I P 1971 *Theory of Lattice Dynamics in the Harmonic Approximation* (New York: Academic)
[33] Bhatia A B and Thorton D E 1970 *Phys. Rev.* B **2** 3004
[34] Lucchini M U and Nex C M M 1987 *J. Phys. C: Solid State Phys.* **20** 3125
[35] Hafner J 1983 *J. Phys. C: Solid State Phys.* **16** 5773
[36] Hafner J 1983 *Phys. Rev.* B **27** 678
[37] Los J and Janssen T 1990 *J. Phys.: Condens. Matter* **2** 9553
[38] Janot C, de Boissieu M, Dubois J M and Pannetier J 1989 *J. Phys.: Condens. Matter* **1** 1029
[39] Suck J B 1993 *Proc. 8th Intern. Conference on Liquid and Amorphous Metals* ed J Hafner (*J. Non-Cryst. Solids* (in print))
[40] Henley C L 1987 *Comm. Condens. Matter Phys.* **13** 59
Bacon G E 1972 *Acta Crystallogr.* A **28** 357
[41] Hafner J and Krajčí M 1993 *Phys. Rev.* B in print
[42] Hafner J 1983 *Proc. 2nd Int. Conf. on the Structure of Noncrystalline Solids* ed P H Gaskell, J M Parker and E A Davies (London: Taylor and Francis) p 539
[43] Srolovitz D, Egami T and Vitek V 1981 *Phys. Rev.* B **24** 6936
[44] Karpov V G, Klinger M I and Ignatiev F N 1983 *Zh. Eksp. Theor. Fiz.* **84** 760 (Engl. transl. *Sov. Phys.–JETP* **57** 439)
[45] Buchenau U, Galperin Yu M, Gurevich V L and Schober H R 1991 *Phys. Rev.* B **43** 5039
[46] Laird B B and Schober H R 1991 *Phys. Rev. Lett.* **66** 636
Schober H R, Oligschleger C and Laird B B 1993 *Proc. 8th Int. Conf. on Liquid and Amorphous Metals* ed J Hafner (*J. Non-Cryst. Solids* (in print))
[47] Nelson D R 1983 *Phys. Rev.* B **28** 5515
Nelson D R 1990 *Solid State Physics* **41** 1